JOURNAL OF APPLIED BIOMECHANICS, 2000, **16**, 36-51

Modeling the Stiffness Characteristics of the Human Body While Running With Various Stride Lengths

Timothy R. Derrick, Graham E. Caldwell, and Joseph Hamill

A modified mass-spring-damper model was used to simulate the vertical ground reaction forces of a human runner as stride length was altered. Spring stiffness values were selected by an optimizing routine that altered model parameters to match the model ground reaction force curve to a runner's actual ground reaction force curve. A mass in series with a spring was used to simulate the behavior of body structures that produce the active portion of the ground reaction force. A second mass in series with a spring-damper system was used to simulate the behavior of those components that cause the impact portion of the ground reaction force. The stiffness of the active spring showed a 51% decrease as subjects increased their stride length. The stiffness value of the impact spring showed a trend opposite that of the active spring, increasing by 20% as strides lengthened. It appears that the impact stiffness plays a role in preventing the support leg from collapsing in response to the increased contact velocities seen in the longer strides.

Key Words: running impacts, optimization, ground reaction forces, lower extremity

Introduction

The vertical ground reaction force (GRF) profile of the running stance phase of heel-toe runners is characterized by an early impact peak (passive phase) as the foot collides with the ground. This is followed by a second peak (active phase) as downward motion of the body's center of mass (CM) is arrested and reversed (Bobbert, Schamhardt, & Nigg, 1991; Cavanagh & Lafortune, 1980). Active muscles and passive structures such as the shoe, heel pad, bone, and cartilage act together to absorb and then generate mechanical energy during this support phase. Modeling of the running motion has given insight to general mechanisms of energy fluctuations, such as the "bouncing ball" theory in which the body successively stores and then releases the stored energy during the running cycle (Cavagna, Heglund, & Taylor, 1977). This model is consistent with the in-phase CM

T.R. Derrick is with the Department of Health and Human Performance at Iowa State University, Ames, IA 50011. G.E. Caldwell and J. Hamill are with the Department of Exercise Science at the University of Massachusetts, Amherst, MA 01003.

kinetic and potential energy changes during running (Cavagna, Thys, & Zamboni, 1976).

These energy characteristics can be predicted using mass-spring (MS) models in which the spring element is used to simulate both energy absorption and generation associated with the motion of the total body mass (Cavagna, Franzetti, Heglund, & Williams, 1988; Farley & Gonzalez, 1996). These models use the energy storage characteristics of the spring to simulate energy absorption in the body, and they use the energy restoration characteristics to simulate energy generation in the body. They have proven useful for understanding the basic shape of the active portion of the vertical GRF curve (McMahon, Valiant, & Frederick, 1987).

Alexander, Bennett, and Ker (1986) presented four models composed of various configurations of masses, springs, and dampers in order to investigate the mechanical properties of mammalian paw pads. These authors found that the initial impact phase of the GRF cannot be well-predicted by a simple MS model. This view was supported by evidence from Bobbert et al. (1991) that suggested that the impact phase was an independent phenomenon associated with support leg motion. Thus, a mass-spring-damper model (MSD) similar to the one used by Alexander et al. (1986) was used in the present investigation in order to satisfactorily predict both active and passive phases. The purpose of this study was to investigate the stance phase in running using a modified MSD model. Our hypothesis was that a modified MSD model could replicate the vertical GRF profile across a range of stride length/stride frequency combinations while running at a constant speed. If the body behaves as a mass-spring model would predict, then this protocol will result in shorter contact times and thus an increased vertical stiffness during running with shorter stride lengths (McMahon et al., 1987).

Methods

Overview of Modeling Approach

The approach we took in this study was a mixture of experimental and modeling techniques. After collecting real vertical GRF (RGRF) data from subjects running at a constant velocity while stride length was manipulated, we constructed a modified MSD model capable of generating model vertical GRF (MGRF) profiles. The model parameters were investigated with a sensitivity analysis to understand their effect on various aspects of the MGRF curves. Finally, the model parameters were optimized at each stride length to give the best fit between RGRF and MGRF profiles. The variation of model parameters as a function of stride length was then analyzed and discussed.

Experimental Protocol

Ten healthy male recreational runners participated in the study. Average age, height, mass, and preferred stride lengths were 27 ± 5 years, 179 ± 5 cm, 76 ± 12 kg, and 2.85 ± 0.15 m, respectively. After reading and signing an informed consent document in accordance with university policy, the subjects were asked to warm up by running along a 30-m runway at 3.83 m · s^{-1}. The velocity was monitored using two infrared switches connected to a timer. During this warm-up, each subject's preferred stride length (PSL) was calculated. The subjects then ran in five stride-length conditions: PSL ± 20% of PSL and ± 10% of PSL, using runway markers to help attain the correct stride length. Each subject completed a minimum of five successful trials (within 5% of 3.83 m · s^{-1}) for

each stride length condition. The condition order was balanced across the 10 subjects. The motion of retroreflective markers on the hip, knee, ankle, and fifth metatarsal joints were videotaped at 200 Hz and digitized using a Motion Analysis VP 110 processor. Support leg center of mass was calculated using the anthropometric model in Vaughan, Davis, and O'Connor (1992).

The vertical GRF from an AMTI force platform was sampled at 1000 Hz using a 12-bit analog-to-digital converter. The kinematic and kinetic data were synchronized by a pulse to the analog-to-digital converter that simultaneously illuminated an LED in the field of view of the camera. Force values greater than 100 N above the baseline were saved for comparison to the MGRF curves. This relatively high threshold value was chosen to reduce the nonlinear regions at the start and end of the RGRF curves.

The MSD Model

The equations for the vertical motion of the MSD model (Figure 1) are:

$$A_1 = (K_1 / M_1) \cdot (P_2 - P_1) + g \quad (1)$$

$$A_2 = -(K_2 / M_2) \cdot P_2 - (K_1 / M_2) \cdot (P_2 - P_1) - C / M_2 \cdot V_2 + g \quad (2)$$

where M_1 is the point mass of the upper element; M_2 is the point mass of the lower element; P_1, V_1, and A_1 are the vertical position, velocity, and acceleration of M_1; P_2, V_2, and A_2 are the vertical position, velocity, and acceleration of M_2; K_1 is the linear spring constant of the massless upper spring; K_2 and C are the linear spring constant and damping coefficient of the massless lower spring and damper, respectively; and g is the acceleration due to gravity ($-9.81\ m \cdot s^{-2}$). These equations are discussed in Alexander et al. (1986). The equations were numerically integrated twice using an Euler method with a time step of 0.0001 s to obtain velocities and positions. Finally, the MGRF curve was calculated by adding the force in the lower spring and the force in the damper element:

$$\text{MGRF} = (K_2 \cdot P_2) + (C \cdot -V_2) \quad (3)$$

Bobbert, Schamhardt, and Nigg (1991) successfully used a method of decomposing the vertical GRF into the contributions of the support leg and the rest of the body. The impact portion of the curve was constructed from the support leg center of mass acceleration. They concluded that the impact peak was primarily caused by the deceleration of the support leg. The masses used in the present model were initially calculated to approximate the support leg (M_2) and the rest of the body (M_1). The optimization routine was performed on a subset of the data and was allowed to adjust these values until an optimal fit was found between the VGRF and MGRF curves. It was found that the best fits were obtained with the lower mass (M_2) at approximately 20% of the total mass of the runner. This value was then used as a constant for the entire optimization procedure. Typically, support leg masses are somewhat less than this value (16%, Winter, 1992), but the exact portion of the body mass responsible for the impact is difficult to estimate.

A_1 and A_2 were both given initial values of $-9.81\ m \cdot s^{-2}$ for all stride length conditions. Initial V_1 and V_2 values were estimated from measured values because stride length will influence contact kinematics. The kinematic data were used to calculate the support leg center of mass velocity at heel contact as an estimate of V_2 at contact. The

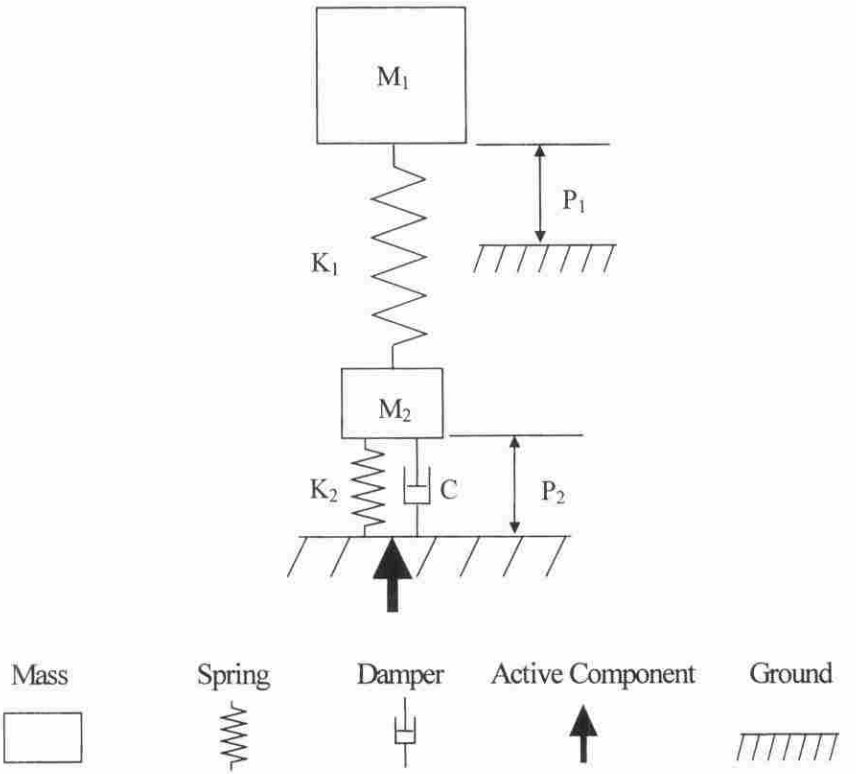

Figure 1 — Schematic diagram of the modified mass-spring-damper model.

initial V_1 value was derived by calculating the vertical CM contact velocity using the impulse momentum relationship applied to the RGRF minus the velocity due to the momentum of the support leg. This insured that the momentum of the model at contact was always equal to that of the runner.

The damper shown in Figure 1 produced force as a function of velocity. Because the lower spring experienced a sudden change in length at contact, a relatively large force was produced. The lower spring was stretched at contact so that the force caused by K_2 opposed the damper force, and the net MGRF was then near zero at contact as in the RGRF. The damping ratio is a useful non-dimensional measure of damping (Smith, 1988) that is calculated by dividing the damping coefficient by the critical damping coefficient $[2(K_2M_2)^{.5}]$. Various coefficients between 0.15 and 0.55 were tried in an effort to get the model's force contribution from the lower mass to be similar to the support leg contribution calculated by Bobbert et al. (1991). A damping ratio of 0.35 was selected and held constant during the optimization procedure. This value was also used by Alexander et al. (1986) in their MSD model of paw pads. Özgüven and Berme (1988) reported that damping ratio values found in the literature ranged from 0.20 to 0.67 for various activities.

For each stride length, the downhill simplex method of multidimensional optimization (Press, Flannery, Teukolsky, & Vetterling, 1989) was used to find the values for K_1,

K_2, and P_2 that gave the best fit between RGRF and MGRF curves. Repeated convergence from different starting positions assured location of a global minimum of this optimizing function. More detail concerning the optimizing function is shown in the appendix.

Repeated measures analyses of variance were performed to compare model values between stride length conditions. Tukey multiple comparison tests for polynomial contrasts were calculated when appropriate.

Results

Experimental Trials

Several characteristics of the RGRF curves (Figure 2) changed as stride length decreased. On average, the impact peak decreased in magnitude from 2.39 BW to 1.59 BW and its time of occurrence increased from 28.8 ms to 34.1 ms as stride length changed from +20% PSL to –20% PSL. The average active peak also decreased in magnitude from 2.92 BW to 2.44 BW from +20% PSL to –20% PSL. Longer stride lengths were associated with longer stance times (243.0 ms for the +20% condition vs. 228.0 ms for the –20% condition). These differences resulted in decreasing average impulse values (331.6 N · s to 238.7 N · s) as stride length changed from +20% PSL to –20% PSL.

Sensitivity Analysis

In order to demonstrate the effects of model components, a sensitivity analysis was performed on selected variables (Figure 3) and initial conditions (Figure 4). In the case of variables optimized in the subsequent modeling of running stride length (K_1, K_2, and initial P_2) or calculated from the human subjects (initial V_1 and initial V_2), the range was determined from the 250 modeled trials. For variables held constant during optimization (M_2 ratio and the damping ratio), ranges were selected that encompassed realistic values for that variable and centered on the constant value used during the optimization. Variables other than the one being varied were given mean values from the modeled trials.

Because the two springs were in series, changing their stiffness values had similar effects. The stiffness of the upper spring (K_1) had its greatest effect on the active portion of the MGRF curve (Figure 3a), influencing both timing and magnitude. As K_1 increased, the duration of the MGRF curve decreased from 320 to 161 ms (K_1 range, 15 to 65 kN · m^{-1}). The time to the impact peak remained relatively unaffected, but the active peak occurred earlier as the value of K_1 increased. Stiffer K_1 values also resulted in greater magnitudes for both peaks.

The stiffness values for the lower spring (K_2) affected the impact peak more than the active peak (Figure 3b). As K_2 increased (54.5 to 166.7 kN · m^{-1}), the impact peak increased in magnitude, and its time from initial contact decreased. Active peak amplitude increased slightly, and its time of occurrence became earlier as K_2 increased. The effect of higher K_2 stiffness on model stance time was less dramatic than that for K_1 (257 to 186 ms).

The M_2 ratio is the mass of the lower element, expressed as a proportion of the total mass. Increasing this proportion from 0.12 to 0.28 increased both the magnitude and timing of the impact peak (Figure 3c), primarily due to the greater momentum of M_2 and thus higher spring deformation at foot contact. Distributing more mass to M_2 also decreased the model stance time slightly because the lower spring was stiffer than the upper one. During the subsequent optimization, the M_2 ratio was given a constant value of 0.20.

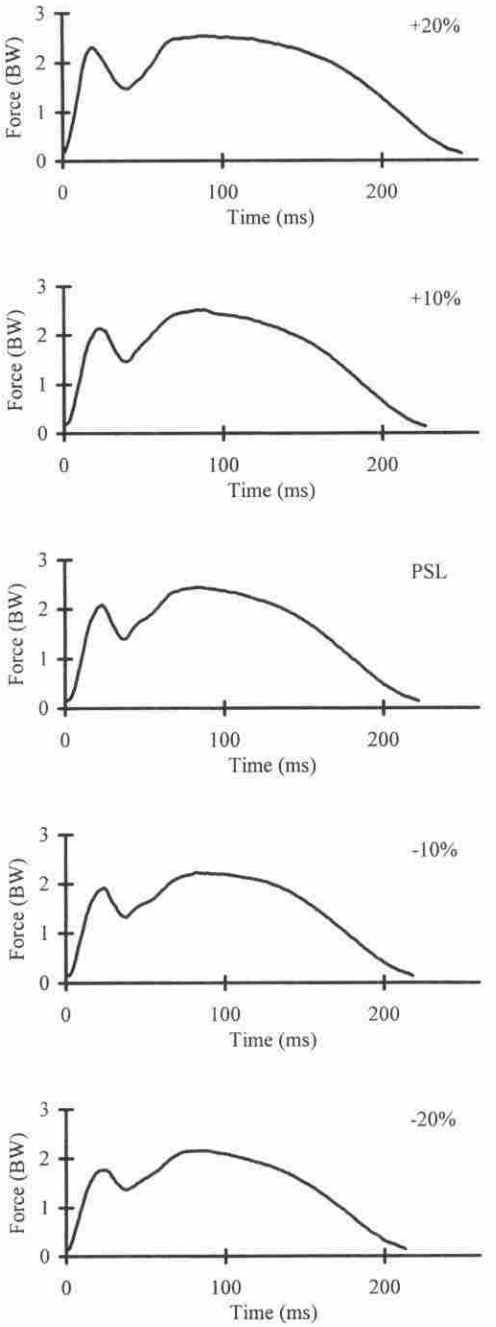

Figure 2 — Typical RGRF curves for one trial of each stride length condition of a single subject. Force is measured in multiples of bodyweight (BW).

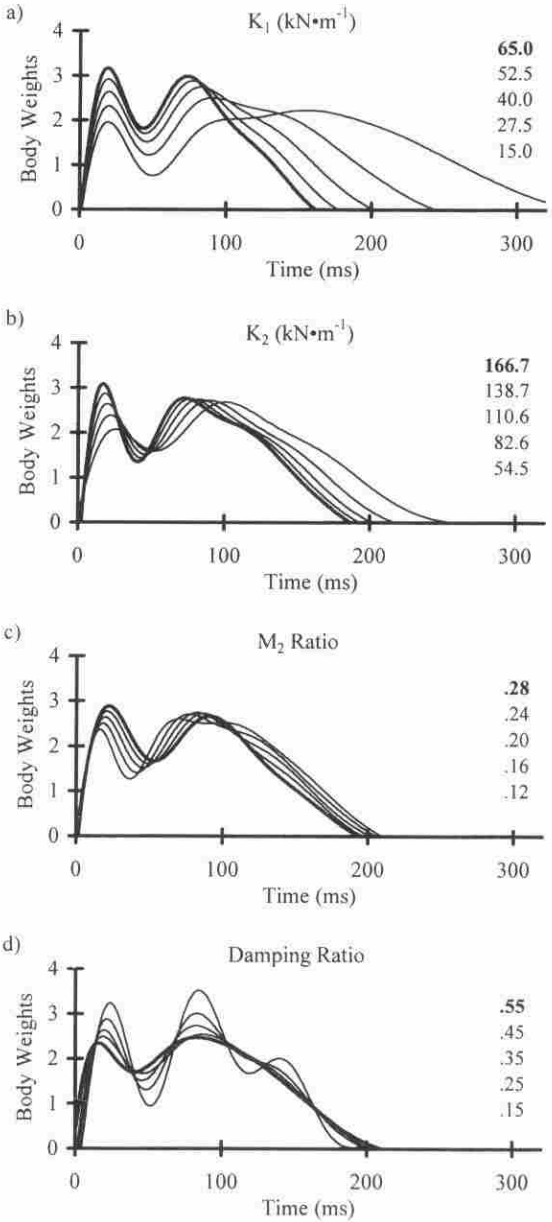

Figure 3 — The sensitivity of the model to upper spring stiffness (K_1), lower spring stiffness (K_2), the ratio of the lower mass to the total mass (M_2 ratio) and the damping ratio. Numeric values listed on each graph indicate the magnitude of the given variable. Increasing K_1, K_2, and M_2 ratio values correspond to increasing impact peak values. Increasing damping ratio values correspond to decreasing impact peak values. Force is measured in multiples of body-weight (BW).

The main effect of the damper was to eliminate "chatter" in the lower spring, which could cause M_2 to bounce during the stance phase (Alexander et al., 1986). In addition to the desired effect, increasing the damping ratio decreased the impact peak and the time from contact to the impact peak (Figure 3d).

The model was also sensitive to initial conditions (Figure 4). The position of the lower mass at contact (P_2) influenced the magnitude and timing of the impact peak and the initial MGRF value (Figure 4a). Increasing P_2 stretched the lower spring and compressed the upper spring, resulting in a net downward force because the lower spring was stiffer. As this downward force countered the undesired damper force caused by the sudden impact, increasing P_2 decreased the magnitude of the MGRF curve at contact. The extra energy stored in the lower spring was released after contact, resulting in greater but delayed impact peaks.

The initial velocity of the upper mass (V_1) was critical in determining the magnitude of the active peak and the stance time (Figure 4b). Initial V_1 values that were too small could result in insufficient stored spring energy for the model to leave the ground (note the two lowest V_1 values in Figure 4b). A greater initial velocity resulted in greater spring deformation and more stored energy. Therefore, as the magnitude of initial V_1 increased from –0.25 to –1.05 m/s, the magnitude of the active force peak increased and stance time was reduced. A smaller increase was seen in the magnitude of the impact peak.

In contrast, the initial velocity of the lower mass (V_2) affected both the time and magnitude of the impact peak (Figure 4c). As the magnitude of initial V_2 increased, the lower spring deformed more and reached maximal deformation and thus peak force earlier. Increasing initial V_2 had the additional effect of increasing the velocity-dependent damper force and therefore increasing the initial force at contact.

Model Optimization

Since the optimization procedures were designed to have the MGRF curves mimic the RGRF, it was important that the areas under the two curves be similar. However, the damper absorbed energy that was not returned to the system, and without adjustment this would cause an underestimation of the MGRF impulse. To offset this energy loss, the model was modified by the insertion of an active component (Figure 1). In the body, energy can be altered by the activation of muscles. This results in an increase in the ground reaction forces and an increase in the vertical impulse. In order to simulate this process the vertical force value was increased by 10% at every point on the MGRF curve. For the typical case the unadjusted MGRF impulse was 212.3 N · s compared to the RGRF impulse of 232.2 N · s (Figure 5a). After adjustment of the MGRF impulse by 10% (to 233.5 N · s), the mean squared error (MSE) between the curves in this example decreased from 0.037 BW^2 to 0.009 BW^2 (Figure 5b).

Figure 6 shows typical RGRF and MGRF curves of a single subject, while Table 1 presents the average MSE values from each stride length condition. The average MSE value for all conditions was 0.049 BW^2, with the +20% condition having the highest value (0.068 BW^2). This relatively large value was due to a single subject who displayed very high impact peaks during this condition. In these trials the impact peak was accurately modeled but the minimum value between the two peaks was underestimated. Omitting this subject's trials reduced the MSE to 0.046 BW^2, consistent with the other conditions.

The average absolute difference in impulse between all of the RGRF and MGRF curves was 6.99 N · s or 2.5%. This impulse difference was greatest during the +20% con-

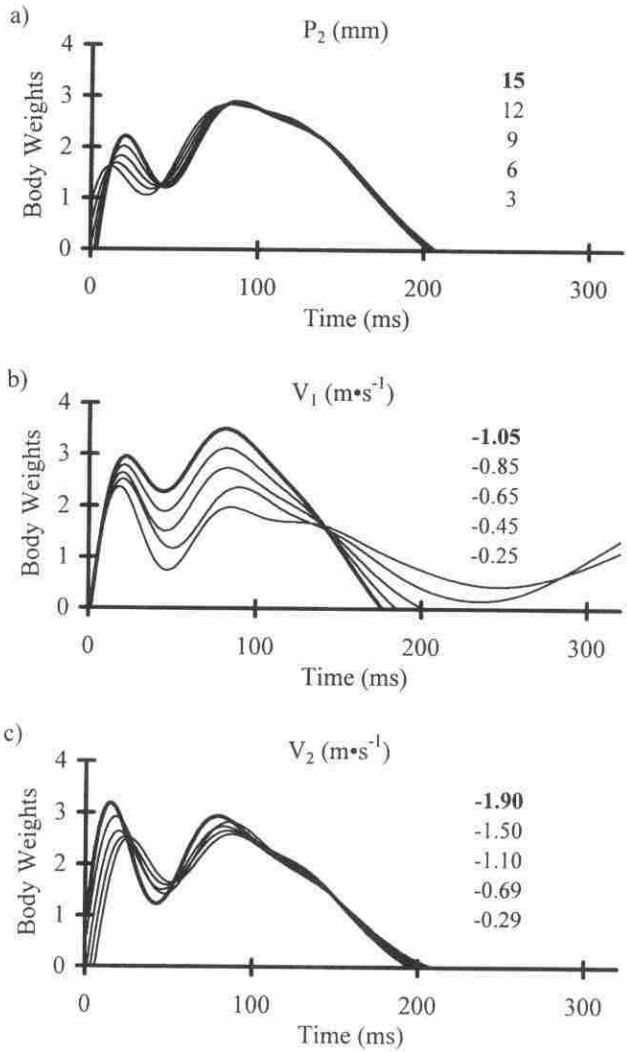

Figure 4 — The sensitivity of the model to the initial values of the position of the lower mass (P_2), the velocity of the upper mass (V_1), and the velocity of the lower mass (V_2). Numeric values listed on each graph indicate the magnitudes of the given variable. Increasing P_2, V_1, and V_2 values correspond to increasing impact peak values. Force is measured in multiples of bodyweight (BW).

dition (8.5 N · s) and least during the –20% condition (5.5 N · s). Since the CM contact velocity of the runner was the same as the model's and the impulses were roughly equal, the model and runner are absorbing and generating the same amount of energy, and the CM velocity when each system leaves the ground at the end of stance will be the same.

Finally, the rate of loading was an important factor in assessing the fit of the model to the actual data because this parameter was sensitive to the lower spring stiff-

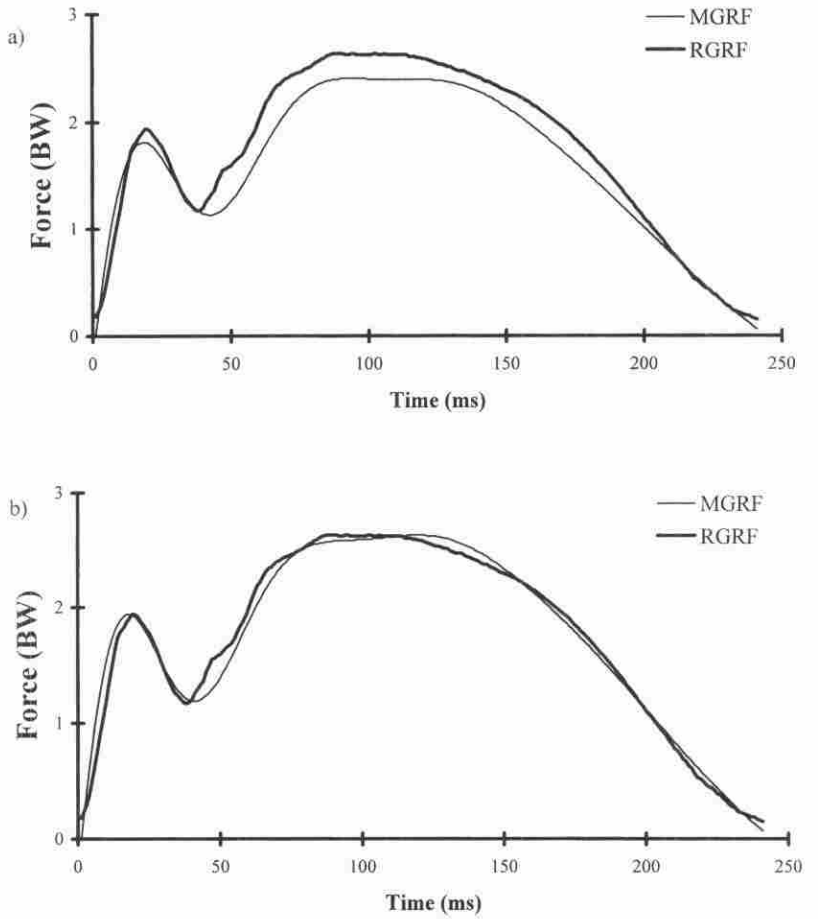

Figure 5 — Comparison of RGRF and the MGRF showing the need to add energy to the model to compensate for the energy lost in the damper: (a) unmodified model underestimates the RGRF; (b) a 10% force adjustment enables a better fit. Force is measured in multiples of bodyweight (BW).

ness value. The slope between 20% and 80% of the impact peak was calculated, with an average absolute difference between RGRF and MGRF curves of 4.3 BW · s^{-1} (4.7%). This difference in slope was greatest during the +20% condition (5.6 BW · s^{-1}) and least during the –20% condition (3.0 BW · s^{-1}).

Stiffness and Stride Length

Shorter stride lengths (more frequent strides) require shorter stance times, and the model was able to replicate the same range of stance times as in the experimental data (243 ms during the +20% condition to 227 ms during the –20% condition). According to Figure 3a, shorter stance times can be accomplished by increasing the upper spring stiffness K_1,

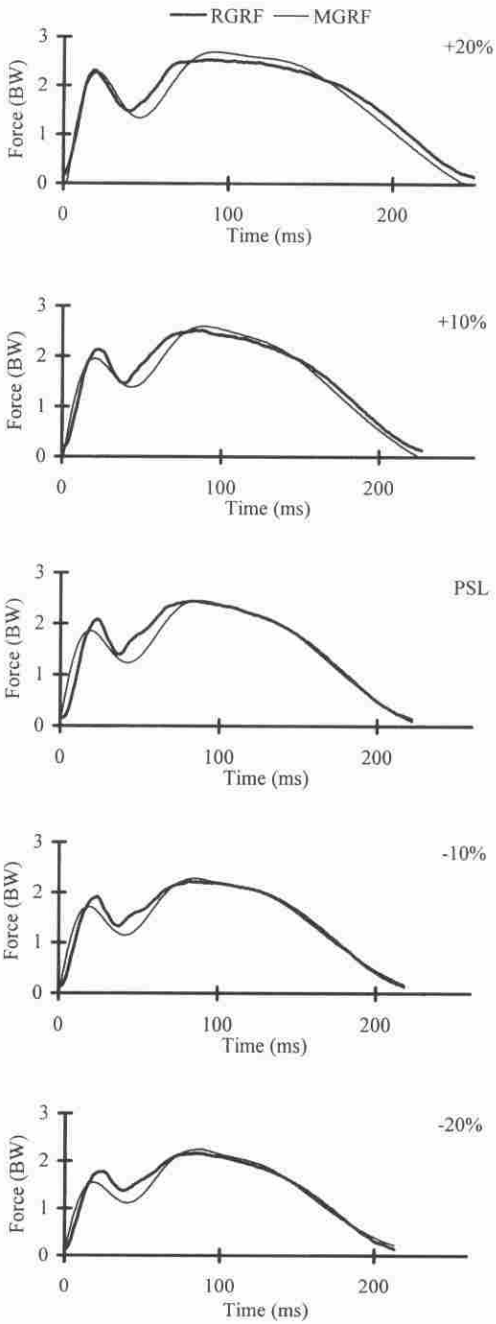

Figure 6 — Typical fits between RGRF and MGRF curves for one trial of each stride length condition of a single subject. Force is measured in multiples of bodyweight (BW).

Table 1 Model Results Showing the Influence of Stride Length on the Stiffness of the Upper Spring (K_1), the Stiffness of the Lower Spring (K_2), the Position of the Lower Mass at Contact (P_2), the Velocity of the Upper Mass at Contact (V_1), and the Velocity of the Lower Mass at Contact (V_2)

Stride Length	K_1 (kN · m^{-1})	K_2 (kN · m^{-1})	P_2 (mm)	V_1 (m · s^{-1})	V_2 (m · s^{-1})	MSE (BW^2)
+20%	25.8	100.7	9.9	–1.00	–1.04	0.068
+10%	29.5	91.1	8.6	–0.85	–0.85	0.048
PSL	34.1	78.4	7.4	–0.73	–0.66	0.042
–10%	42.4	78.2	6.1	–0.55	–0.65	0.043
–20%	52.6	83.9	5.0	–0.44	–0.63	0.049

Note. The mean squared error (MSE) indicates the average degree of fit between the RGRF curve and the MGRF curve.

and this was the result from the optimization procedure (Table 1 and Figure 7). Polynomial contrasts indicated significant linear ($p = .0001$) and second order ($p = .01$) trends across stride length conditions. However, increasing K_1 also tends to increase the impact peak value, while the model shows this peak decreasing from 2.4 BW to 1.6 BW from the +20% to –20% stride length conditions. This suggests that the lower spring must have offset this effect as stride length decreased.

In contrast, the stiffness of the lower spring (K_2) decreased with decreasing stride length (Table 1 and Figure 7). Again, there were significant linear ($p = .01$) and second order ($p = .05$) trends to K_2 as a function of stride length. The sensitivity analysis illustrated that this reduced K_2 stiffness (Figure 3b) is the cause of the lower impact peaks with decreased stride length. The reduced contact velocity of the lower mass at the shorter stride lengths (V_2 in Table 1, and see Figure 4c) amplifies this effect. Also, the slope prior to the impact peak was greatest during the –20% condition (127.6 BW · s^{-1}) and least during the +20% condition (77.3 BW · s^{-1}). Again, this reduced slope can be

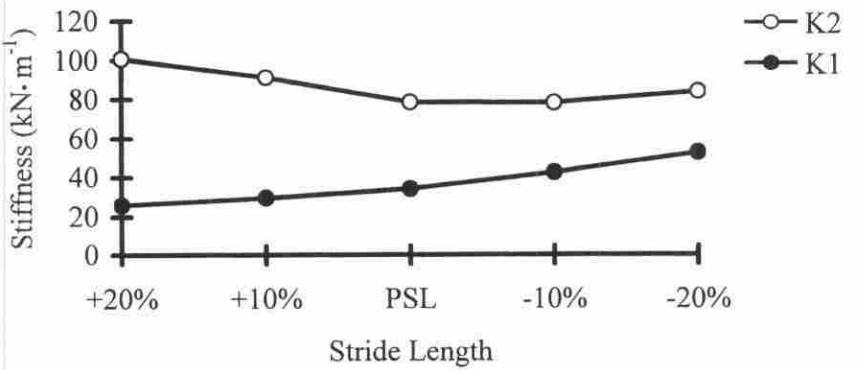

Figure 7 — Results of the model showed that the upper spring became stiffer (K_1) as stride length decreased, while the lower spring tended to become more compliant (K_2).

explained by the reduced K_2 stiffness (Figure 3b). Finally, the reduced contact velocities (V_2) at shorter stride lengths would produce lower damper forces and therefore smaller counteracting forces with lower initial P_2 values (Table 1). This reduction in P_2 values would cause a decrease in the impact peak and the slope of the impact peak (Figure 4a). Therefore the changes in K_2 with stride length may be underestimated due to the inclusion of this artificial constraint.

Discussion

The experimental results of this study indicate that decreases in stride length reduce both the stance time and the magnitude of the impact peak. The MSD model with the active component was able to replicate these experimental GRF patterns and responded to stride length changes in the same manner as did the running subjects. The upper spring stiffness K_1 was always less than lower spring stiffness K_2. Further, K_1 increased with shorter stride lengths, while K_2 decreased. Therefore we accept our hypothesis that the modified MSD model is a suitable representation of the running behavior across a range of stride lengths.

The human body is a complex machine with multiple degrees of freedom available to accomplish any single task. In the face of this complexity, one analysis strategy is to simplify the system through a model that contains only the most salient features of the behavior. If the model is too simple, it will not accurately portray the phenomenon; an overly complex model will cause interpretation problems. The MSD model was simple, reproduced actual vertical GRFs, and allowed us to gain insight regarding the stiffness characteristics of the body during running. The upper mass-spring system, which controlled the active portion of the GRF curve, doubled the stiffness of its spring as stride length was decreased (Table 1 and Figure 7). The lower mass-spring-damper system controlled the impact portion of the GRF curve, and its stiffness value showed the opposite trend, increasing with shorter stride lengths.

McMahon and Cheng (1990) differentiated vertical stiffness (k_{vert}) from leg stiffness (k_{leg}) based on the angle of the lower extremity with respect to the vertical. The k_{vert} variable assumes a vertical spring, while the k_{leg} variable assumes a spring with the same orientation as the lower extremity. Unless the springs are parallel, k_{vert} will be greater than k_{leg}. Cavagna et al. (1988) and McMahon et al. (1987) demonstrated that k_{vert} increases with running velocity, but when McMahon and Cheng (1990) took into account the changing orientation of the lower extremity during the stance phase, they found that k_{leg} did not change with running velocity. However, stiffness does not appear to remain constant with changes in stride length (or stride frequency). Farley and González (1996) found a 2.3 fold increase in k_{leg} using a range of stride frequencies between 26% below and 36% above the preferred stride frequency. In the current study, there was a 2.0 fold increase in K_1 between stride frequencies 20% below to 20% above the preferred. Slightly higher stiffness values found in this study may reflect the measurement of k_{vert} rather than k_{leg} or the discrepancy may be due to the inclusion of the lower mass-spring-damper element. The damper produces a force opposite to that of the upper spring. Thus, stiffer K_1 values were required to counter the damping force.

The MSD model differs from these mass-spring models by virtue of the inclusion of elements that lead to insight concerning the impact as well as the active portions of the vertical GRF. With longer stride lengths the vertical contact velocity increased. In order to keep the support leg from collapsing under this increased momentum, the body increased the stiffness associated with the leg mass (K_2). Control of this stiffness could

be managed in two ways: reorientation of the support leg geometry (Gerritsen, Bogert, & Nigg, 1995) or by changing the activation of the lower extremity musculature (Bobbert, Yeadon, & Nigg, 1992). Support leg geometry influences stiffness by changing the perpendicular distance from the ground reaction force vector to the joint center. If this line of action is directed through the joint centers, shock attenuation will be transferred from active muscle to passive structures, which may not be able to attenuate as much shock (Derrick, Hamill, & Caldwell, 1998). For the period prior to the impact peak, the perpendicular distance of the GRF line of action behind the knee joint center (D_k) increased ($p < .05$) from 3.1 to 5.4 cm as the stride length decreased from +20% to –20% PSL. This suggests that the knee was stiffest during the longer stride length condition. At peak impact this trend was reversed, with the knee joint geometrically more compliant during the long stride length condition.

At first, these results appear contrary to those found by Lafortune, Hennig, and Lake (1996). These researchers examined the role of initial knee angle on the regulation of leg stiffness using a human pendulum protocol. They concluded that the knee joint did not play a role in the regulation of initial leg stiffness. This discrepancy originates from differences in protocol. Lafortune et al. kept the orientation of the leg to the force platform horizontal (perpendicular to the wall mounted force platform). Since their human pendulum produces predominantly normal GRF forces, neither the force vector nor the knee joint location changed as the knee angle was altered. Thus D_k was held constant in their study. Since we hypothesize that changes in the stiffness at the knee are due to changes in D_k, it would be reasonable to predict no changes in initial leg stiffness if D_k is held constant. This is exactly what Lafortune et al. found.

In terms of anatomical structures associated with these stiffness values, the upper spring requires large adjustments and needs the ability to absorb and generate large amounts of energy, implicating muscular involvement. The structures represented by the lower spring must deform rapidly in a viscoelastic manner upon impact and require less capability for adjustment. Most of these requirements would be fulfilled by the ground/shoe interface (Kim, Volshin, & Johnson, 1994), heel pad, articular cartilage, and bone (Cavanagh, Valiant, & Misevich, 1984). Functionally, rapid pronation immediately after heel contact may also play a role in spring compliance (Denoth, 1983). Future studies should examine the relative contributions of muscles and passive components to total body stiffness.

Studies indicate a shock attenuation benefit but a metabolic energy cost associated with a compliant support leg. McMahon et al. (1987) determined that "Groucho" running (with exaggerated knee flexion) was more compliant than normal running, but metabolic energy costs were substantially higher. Running with longer stride lengths produced greater compliance of the support leg (Farley & González, 1996) and also leads to increased oxygen consumption (Cavanagh & Williams, 1982; Hamill, Derrick, & Holt, 1995). However, both McMahon et al. (1987) and Hamill et al. (1995) demonstrated increased shock attenuation with these more compliant running styles, understandable in that a compliant spring will transmit less shock than a stiff one. Runners typically select the running style that minimizes oxygen consumption, indicating that this may be a more important optimizing criterion than shock attenuation (Hamill et al., 1995).

The results presented in this study relate only to non-fatigued running of healthy college-aged male recreational runners. With fatigue it might be expected that the stiffness associated with muscles could be altered and the role of passive structures accentuated. Likewise, an injury may result in altered spring stiffness values to relieve load at the

site of the injury. Differences associated with gender and age could also be hypothesized, based on differences in muscle and passive tissue structure (Frontera, Hughes, Lutz, & Evans, 1991; Vandervoort, 1992). Also, elite athletes may optimize their stride length and stiffness based on different criteria than recreational runners. Research into these areas may provide unique insight into both the kinematics and control of human running.

References

Alexander, R. McN., Bennett, M.B., & Ker, R.F. (1986). Mechanical properties and function of the paw pads of some mammals. *Journal of Zoology* (London), **209**, 405-419.

Bobbert, M.F., Schamhardt, H.C., & Nigg, B.M. (1991). Calculation of vertical ground reaction force estimates during running from positional data. *Journal of Biomechanics,* **24**, 1095-1105.

Bobbert, M.F., Yeadon, M.R., & Nigg, B.M. (1992). Mechanical analysis of the landing phase in heel-toe running. *Journal of Biomechanics,* **25**, 223-234.

Cavagna, G.A., Franzetti, P., Heglund, N.C., & Williams, P. (1988). The determinants of the step frequency in running, trotting and hopping in man and other vertebrates. *American Journal of Physiology,* **399**, 81-92.

Cavagna, G.A., Heglund, N.C., & Taylor, C.R. (1977). Mechanical work in terrestrial locomotion: two basic mechanisms for minimizing energy expenditure. *American Journal of Physiology,* **233**, R243-261.

Cavagna, G.A., Thys, H., & Zamboni, A. (1976). The sources of external work in level walking and running. *Journal of Physiology,* **262**, 639-657.

Cavanagh, P.R., & Lafortune, M.A. (1980). Ground reaction forces in distance running. *Journal of Biomechanics,* **13**, 397-406.

Cavanagh, P.R., Valiant, G.A., & Misevich, K.W. (1984). Biological aspect of modeling shoe/foot interaction during running. In E.C. Frederick (Ed.), *Sport shoes and playing surfaces* (pp. 24-46). Champaign, IL: Human Kinetics.

Cavanagh, P.R., & Williams, K.R. (1982). The effect of stride length variation on oxygen uptake during distance running. *Medicine and Science in Sports and Exercise,* **14**, 30-35.

Derrick, T.R., Bates, B.T., & Dufek, J.S. (1994). Comparative evaluation of time-series data sets using the Pearson product-moment correlation coefficient. *Medicine and Science in Sports and Exercise,* **26**, 919-928.

Derrick, T.R., Hamill, J., & Caldwell, G.E. (1998). Energy absorption of impacts during running at various stride lengths. *Medicine and Science in Sports and Exercise,* **30**, 128-135.

Denoth, J. (1983). Load on the locomotor system and modelling. In B.M. Nigg (Ed.), *Biomechanics of running shoes* (pp. 63-116). Champaign, IL: Human Kinetics.

Farley, C.T., & González, O. (1996). Leg stiffness and stride frequency in human running. *Journal of Biomechanics,* **29**, 181-186.

Frontera, W.R., Hughes, V.A, Lutz, K.J., & Evans, W.J. (1991). A cross-sectional study of muscle strength and mass in 45- to 78-yr-old men and women. *Journal of Applied Physiology,* **71**, 644-650.

Gerritsen, K.G.M., Bogert, A.J., & Nigg, B.M. (1995). Direct dynamics simulation of the impact phase in heel-toe running. *Journal of Biomechanics,* **28**, 661-668.

Hamill, J., Derrick, T.R., & Holt, K.G. (1995). Shock attenuation and stride frequency during running. *Human Movement Sciences,* **14**, 45-60.

Kim, W., Voloshin, A.S., & Johnson, S.H. (1994)/ Modeling of heel strike transients during running. *Human Movement Sciences,* **13**, 221-244.

Lafortune, M.A, Hennig, E.M., & Lake, M.J. (1996). Dominant role of interface over knee angle for cushioning impact loading and regulating initial leg stiffness. *Journal of Biomechanics,* **29**, 1523-1529.

McMahon, T.A., & Cheng, G.C. (1990). The mechanics of running: How does stiffness couple with speed? *Journal of Biomechanics,* **23**, 65-78.

McMahon, T.A., Valiant, G., & Frederick, E.C. (1987). Groucho running. *Journal of Applied Physiology,* **62**, 2326-2337.

Nigg, B.M., & Anton, M. (1995). Energy aspects for elastic and viscous shoe soles and playing surfaces. *Medicine and Science in Sports and Exercise,* **27**, 92-97.

Özgüven, H.N., & Berme, N. (1988). An experimental and analytical study of impact forces during human jumping. *Journal of Biomechanics,* **21**, 1061-1066.

Press, W.H., Flannery, B.P., Teukolsky, S.A., & Vetterling, W.T. (1989). *Numerical recipes in Pascal*. New York: Cambridge University Press.

Smith, J.W. (1988). *Vibration of structures*. New York: Chapman and Hall.

Vandervoort, A.A. (1992). Effects of aging on human neuromuscular function: Implications for exercise. *Canadian Journal of Sport Science,* **17**, 178-184.

Vaughan, C.L., Davis, B.L., & O'Connor, J.C. (1992). *Dynamics of human gait*. Champaign, IL: Human Kinetics.

Winter, D.A. (1990). *Biomechanics and motor control of human movement*. New York: John Wiley & Sons.

Appendix

The optimizing function consisted of several variables that quantified the differences in timing and magnitude between the RGRF curve and the MGRF curve. Critical difference variables included the first points of the curves (F_{first}), the slope between 20% and 80% of the first peak (F_{slope}), the first peak (F_{p1}), the minimum value between the two peaks (F_{min}), the second peak (F_{p2}), and the last points of each curve (F_{last}). In addition, the difference in the time that the first peak occurred (TF_{p1}) was included. All of these difference values were squared, and coefficients were added to increase or decrease the sensitivity of each variable. Force values were in body weights and time in milliseconds. The sum of these difference values was multiplied by $(1.0–r^2)$ to further account for timing differences between the curves (Derrick, Bates, & Dufek, 1994). The following formula represents the critical function (CF) that was minimized by the optimizing routine:

$$CF = (1.0–r^2) \cdot [\,(0.2 \cdot F_{first}) + (0.1 \cdot F_{slope}) + (1.0 \cdot F_{p1}) + (1.0 \cdot F_{min}) + (0.2 \cdot F_{p2}) + (1.0 \cdot F_{last}) + (20.0 \cdot TF_{p1})]$$

Each difference variable represents the squared difference between the MGRF and RGRF curves.